FULL LENGTH PAPER

TRANSPORT EQUATION TRANSITION MODELING IN CERANS FOR HYPERSONIC FLOWS

R. Balasubramanian, K. Anandhanarayanan, R. Krishnamurthy, Debasis Chakraborty
Directorate of Computational Dynamics
Defence Research and Development Laboratory (DRDL)
Kanchanbagh Post, Hyderabad-500 058
Email : bals.cfd@gmail.com

Abstract

Scope of present work covers implementation to validation of the Langtry-Menter two equation γ-$Re_{\theta t}$ Local Correlation based Transition Model (LCTM) in CERANS code for modeling subsonic to hypersonic flow transition. The LCTM is coupled with SST k-ω turbulence model. The governing equations of γ-$Re_{\theta t}$ model is discretized in finite volume framework similar to the RANS model and implicitized using the point Jacobi method. Transition correlations based on freestream as well as local turbulence intensity and critical momentum thickness Reynolds number were integrated with the model, and the code is validated for several standard transition test cases involving low subsonic to hypersonic high enthalpy flows covering a wide range of turbulent intensities.

Keywords: *CERANS, γ-$Re_{\theta t}$ Transition Model, Correlation, Hypersonic Flow, Implementation, Validation*

Introduction

Aerothermodynamic flowfield environment around a hypersonic flight vehicle is strongly influenced by viscous interaction of shock wave and boundary layer. Such interaction thicken the boundary layer leading to formation of viscous shock layer where enhanced surface heating is observed. Depending on upstream conditions and geometry, flow in the shock layer can be partly laminar, transitional as well as turbulent with possible pockets of flow separation and can as well relaminarize downstream. The surface heat loads drastically increase during and after flow transition, which can directly affect the first order design variables such as airframe geometry, material thickness, weight and the conditions of cruise, thereby necessitating additional thermal protection systems, which increase the complexity of overall design. Hence prediction of boundary layer flow transition is a crucial aerothermal design prerequisite for the hypersonic cruise vehicle project.

Rapid progress in development of high fidelity turbulence models, during the decades preceding and succeeding 80s, led to explosive growth in successful application of the Reynolds Averaged Navier Stokes (RANS) modeling, for turbulent flows by the industrial community for wide variety of aerospace problems. An underlying principle that govern RANS modeling is the assumption that the flow is always and almost fully turbulent right from the leading geometric surface of the flight vehicle. This decree is far from the factual scenario that generally flow undergo transition to turbulence from a quite laminar condition through various means and mechanisms that are completely ignored by RANS model.

Though phenomenological modeling of the physics of boundary layer flow transition itself is not important in many cases, it is necessary to at least include a model description of representative transition phenomenon based on existing knowledge base on the subject. As the aerospace flight vehicle designs are refined and optimized for various requirements such as low drag, low noise, high speed, range and maneuverability, high payload and volume fraction per unit weight and cost, fuel efficient engines as well as optimal airframe reinforcements for

Paper Code : V70 N4/ACFD2018-27-2018. Manuscript received on 09 Nov 2018. Reviewed and accepted as a Full Length Contributed Paper on 12 Nov 2018

Paper presented in the 20th Annual CFD Symposium held at Bangalore on 9-10 August 2018

thermal protection system design, considering the effects of flow transition in the initial design stage can fetch significant competitive design advantages.

Modeling Flow Transition

An overview of various approaches to model flow transition in CFD along with the main requirements for a fully CFD-compatible transition model are presented in detail by Pasquale et al. [1]. Since Reynolds averaging correspond to a low pass filter, the frequency content of spatial scales are averaged out as the Reynolds stresses are modeled and the entire spectral information is lost completely. Hence it is necessary to include additional models for activating/deactivating the turbulence production in the transition zone. An easiest approach to predict transition is by allowing the underlying low Reynolds number form of eddy-viscosity turbulence model itself to mimic the process.

Semi Empirical, Intermittency and Correlation Based Methods

Historically, prediction of boundary layer transition was based on empirical approaches in the form of engineering transition correlations developed and extrapolated from simple experiments. Such methods limits itself to identification of the transition onset location and fully turbulent flow is assumed downstream of this single point onset. One of the most popular and widely used transition model is the semi-empirical e^N method based on local linear stability theory [2]. Another popular approach is to use universal intermittency profile 'γ' due to Dhawan and Narasimha [3] defined as the fraction of time the flow becomes turbulent. Some more approaches such as Abu-Ghannam and Shaw [4], Mayle [5] and Suzen et al. [6,7] uses empirical correlations to determine the transition critical Reynolds number where the momentum thickness Reynolds number (Re_θ) at the boundary layer edge is determined and the turbulence model is activated when it exceeds the quantity obtained from the empirical correlation. Though simple to use in a 2D framework involving non-local operations such as search along body-normal grid direction or integration along external streamlines, these methods when coupled with RANS are powerful enough to provide significant improvements to engineering transition prediction.

RANS Based Modeling

In the realm of turbulence closure model itself (LRN-RANS) allowed to predict transition, special calibration of the model is required by modifying wall damping terms of the turbulent transport equations, where the transition behavior is linked directly to sublayer damping terms [8,9]. Though partially successful only for prediction of bypass transition, its success is a mere whimsical coincidence and hence unreliable. In 3D flows, implementation of these models in the modern industrial CFD code pose additional challenges as they depend on computing non-local integral quantities such as the boundary layer momentum thickness within the whole solution domain. Added complexities in the form of unstructured grid as well as parallelization of CFD code based on domain decomposition necessitates implementation of non-trivial, customized algorithms for determination of Re_θ. Such non-compatibility issues renders the semi-empirical and non-local correlation based models unsuitable and impractical for general purpose CFD.

Transport Equation Transition Models

Most of the aerodynamic design analysis requiring transition information rely heavily on experimental correlations despite the naivety of direct implementation to practical problems. Several transport equation transition models based on the concept of intermittency distribution (γ) of Dhawan and Narasimha [3] have been developed coupling γ with the turbulent and non-turbulent regions, such as modifying the eddy viscosity or turbulence production of the underlying turbulence model.

Steelant and Dick [10] model uses a transport equation for intermittency along with turbulent quantities evaluated using k-ε turbulence model. Suzen and Huang [6,7] proposed the transport equation for intermittency to blend the laminar and turbulent regions based on correlations, and coupled it with the SST k-ω turbulence model. Papp and Dash [11] used the compressibility corrected SSGZ k-ε turbulence model with algebraic transition model as well as a transport equation for intermittency. The form of intermittency transport equations presented in these models are different from one another and were calibrated and blended with several correlations, so as to enhance their prediction to separation as well as cross flow transitions. Also these models could not avoid using the non-local variables and hence have limitation in scope for general purpose CFD.

$\gamma - Re_{\theta t}$ Local Correlation Based Transition Model

An alternative to models based on non-local variables is the framework of Local Correlation based Transition Modeling (LCTM) which require only the local flow information to control turbulence production of the eddy viscosity models, for triggering transition process in the boundary layer. Langtry et al. [12,13] developed the $\gamma - Re_{\theta t}$ transition model as a 'framework' for implementation of correlation-based models into general purpose CFD methods. The physics of the transition process is entirely contained in the experimental correlations used in $\gamma - Re_{\theta t}$ model, i.e., the transport equations only mimic and model transition process and do not attempt to predict the phenomenological process. Since the LCTM is purely dependent on experimental correlations, it can be tailored to predict all type of transition mechanisms. Recent developments have enhanced the predictive capability of the $\gamma - Re_{\theta t}$ model for transition mechanism such as natural, bypass, separation-induced, cross-flow as well as relaminarization. In the LCTM framework, an intermittency transport equation is used to trigger the transition process based on transition length and critical momentum thickness Reynolds number. In addition, another equation for transition momentum thickness Reynolds number, $Re_{\theta t}$, is used for avoiding non-local operations introduced by the variables present in the experimental correlations. Since the straightforward evaluation of Re_θ is difficult in unstructured parallel codes, the vorticity Reynolds number Re_v which is linked to Re_θ is used [13]. The maximum value of Re_v is proportional to Re_θ in the boundary layer and hence it is possible to relate $Re_{\theta t}$, through transition onset Re_θ from correlation to Re_v. The main function of this equation is to force the transport variable to follow the value provided by the experimental correlation outside the boundary layer. This information is diffused into the boundary layer by standard diffusion terms, accounting for the effects of large variation in turbulence intensity and pressure gradient.

Governing Equations

Mean Flow Equations

The governing physical model equations are the unsteady compressible RANS equations which describe the conservation of mass, momentum and energy of the flow field and are given by

$$\frac{\partial \rho}{\partial t} + \frac{\partial (\rho u_j)}{\partial x_j} = 0 \tag{1}$$

$$\frac{\partial (\rho u_i)}{\partial t} + \frac{\partial (\rho u_i u_j)}{\partial x_j} = -\frac{\partial p}{\partial x_i} + \frac{\partial \tau_{ij}}{\partial x_j} \tag{2}$$

$$\frac{\partial (\rho E)}{\partial t} + \frac{\partial (\rho H j)}{\partial x_j} = -\frac{\partial \dot{q}_j}{\partial x_j} + \frac{\partial (\tau_{ij} u_i)}{\partial x_j} \tag{3}$$

where, ρ is the fluid density, u is the velocity vector, p is the fluid pressure, τ is the shear stress tensor, $\dot{q}$ is the heat flux, E is the specific energy and H is the specific enthalpy. The above system of equations is closed based on the assumption of perfect gas with the equation of state given by, $p = \rho R T$, where, R is the gas constant and T, the fluid temperature. The fluid is considered Newtonian, hence a linear stress-strain rate relationship for the laminar viscous stresses is considered and the heat flux follows the Fourier assumption, as $\dot{q} = -k \frac{\partial \dot{q}_k}{\partial x_k}$. Turbulence closure is effectuated using the two equation SST k-ω eddy viscosity turbulence model [14] developed by Menter by blending the Wilcox's k-ω and the standard k-ε models.

LCTM Transport Equations

Details of the $\gamma - Re_{\theta t}$ LCTM are available in standard literature [12, 13] and hence not presented here. The two governing conservation equations of the transition model are as follows:

Transport Equation for the Intermittency

The transport equation for intermittency factor γ which is used to locally trigger transition is given by

$$\frac{\partial (\rho \gamma)}{\partial t} + \frac{\partial (\rho u_j \gamma)}{\partial x_j} = P_\gamma - E_\gamma + \frac{\partial}{\partial x_j}\left[\left(\mu + \frac{\mu_t}{\sigma_f}\right)\frac{\partial \gamma}{\partial x_j}\right] \tag{4}$$

Transport Equation for the Transition Momentum Thickness Reynolds Number

The transport equation for transition momentum thickness Reynolds number is designed to infuse the information of turbulent intensity which varies strongly in the flow domain into the boundary layer, as it is in appropriate to

use the freestream values of turbulence intensity and $Re_{\theta t}$. Further it is necessary to account for the history effects of pressure gradient on the transition onset, rather than just considering only the influence of local pressure gradient. It is given by,

$$\frac{\partial(\rho Re_{\theta t})}{\partial t}+\frac{\partial(\rho u_j Re_{\theta t})}{\partial x_j}=P_{\theta t}+\frac{\partial}{\partial x_j}\left[(\mu+\mu_t)\frac{\partial Re_{\theta t}}{\partial x_j}\right] \quad (5)$$

This equation avoids non-location operations required to evaluate $Re_{\theta t}$ from experimental transition correlations which relate transition onset Reynolds number to the freestream turbulence intensity Tu_∞ and treats the $Re_{\theta t}$ as a transported scalar quantity. More details on the production and destruction terms of the LCTM can be referred from [12].

Transition Model Correlations

Subsonic and Transonic Flows

Langtry and Menter: Correlation Correlations for critical momentum thickness Reynolds number $Re_{\theta c}$ and transition length function F_{length} for subsonic and transonic flows are given by

$$Re_{\theta c}=\begin{cases} Re_{\theta t}-(396.035\times10^{-2}+120.656\times10^{-4}Re_{\theta t}+868.230\times10^{-6}Re_{\theta t}^2 \\ -696.506\times10^{-8}Re_{\theta t}^2+174.105\times10^{-12}Re_{\theta t}^4); & [Re_{\theta t}\le 1870] \\ Re_{\theta t}-(593.11+0.482\,[Re_{\theta t}-1870.0]); & [Re_{\theta t}\le 1870] \end{cases}$$

$$F_{length}=\begin{cases} 398.189\times10^{-1}-119.27\times10^{-4}Re_{\theta t}-132.567\times10^{-6}Re_{\theta t}^2; & [Re_{\theta t}<400] \\ 263.404-123.939\times10^{-2}Re_{\theta t}+194.548\times10^{-5}Re_{\theta t}^2- \\ -101.695\times10^{-8}Re_{\theta t}^3; & [400\le Re_{\theta t}<596] \\ 0.5-(Re_{\theta t}-596.0)\times3.0\times10^{-4}; & [596\le Re_{\theta t}<1200] \\ 0.3188; & [1200\le Re_{\theta t}] \end{cases}$$

Hypersonic Flows

Krause Correlation:The values of $Re_{\theta t}$ in hypersonic flow regime can be of the order of 10^5 which is about two orders of magnitude higher than the values at subsonic regime. Hence Langtry and Menter correlations are not valid for hypersonic flows. In order to overcome this, Krause et al. [15,16] developed correlations especially for hypersonic flows which is purely dependent on the freestream turbulence intensity instead of $Re_{\theta t}$. The correlations are:

$Re_{\theta c}=967.34\times Tu_\infty^{-1.0315}$ and

$F_{length}=10.435\times \mathrm{Tu}_\infty^{2.9756}$

Coupling the SST k-ω With $\gamma-Re_{\theta t}$ Models

The original turbulent kinetic energy production and destruction terms of the SST k-ω equation are modified according to Ref.[12] for coupling the LCTM with the turbulence model.

Boundary Conditions

The boundary conditions for the four partial differential equations due to SST k-ω and $\gamma-Re_{\theta t}$ models mainly involves specification of the inflow/freestream and the wall boundary conditions. The k values at the inflow is specified according to the turbulence intensity and the freestream flow velocity as $k_\infty=\frac{3}{2}\left(\frac{Tu_\infty}{100}U_\infty\right)^2$, the specific dissipation rate at the inflow is specified as $\omega_\infty=\frac{\rho_\infty k_\infty}{t_{t\infty}}$. At no-slip wall, turbulent kinetic energy is zero, $k_w=0$ and specific dissipation rate is given by $\omega_w=\frac{60\,\mu_1}{\rho\,\beta_1 d^2}$.

For the transition model, the freestream value of intermittency is $\gamma_\infty=1.0$ and the transition critical momentum thickness Reynolds number, $Re_{\theta t\infty}$ isprescribed based on transition correlations with the freestream turbulence intensity. The Langtry-Menter's zero pressure gradient $Re_{\theta t\infty}$ correlation is used for subsonic flow studies. In case of supersonic or hypersonic flows, values of $Re_{\theta t\infty}=Re_{\theta c\infty}$ is used, respectively based on the Medida et al. [17] or Krause correlation [16]. At no-slip wall, value of intermittency is such that zero normal gradient for γ and $Re_{\theta t}$ i.e., $\partial n/\partial n=0$ and $Re_{\theta t}/\partial n=0$ are specified. At outflow, all variables are extrapolated from the interior domain.

Implementation of LCTM in CERANS

CERANS is a general purpose CFD code [18] for solving compressible RANS equations in cell centered finite volume frame on sequential and MPI parallel com-

puters. The governing equations of the mean flow are solved in the finite volume framework with an edge based data structure, which dexterously harness the potential of the code to handle structured as well as unstructured hybrid grids. The interfacial numerical fluxes for the mean flow equations were evaluated using approximate Riemann solvers such as modified Roe's flux formulae, or AUSM-family flux functions for the convective fluxes and central differencing for the diffusive fluxes. Flow gradients are evaluated based on the weighted least squares method in case of hexahedral grids and the Green-Gauss method for unstructured/hybrid grids. Second order spatial accuracy is used for evaluating the mean flow fluxes and min-max slope limiter is used to preserve monotonicity in regions of discontinuities. The one equation Spalart-Allmaras [19] and the two equation SST k-ω [14] turbulence models were implemented for addressing the turbulence closure problem.

Flow transition is modeled by implementing the framework of LCTM, solving a couple of partial differential equations, viz., for intermittency and transition critical momentum thickness Reynolds number. Numerical discretization of both turbulence and transition models follow procedures similar to the mean flow modeling, however solved by decoupling from the mean flow. Local or global minimum time stepping shall be used for temporal evolution. Convergence to steady state is accelerated with LUSGS or Point Jacobi based implicit procedure for all the equations. The source terms of turbulence and transition models are treated implicitly for alleviating numerical stiffness.

Validation of CERANS for Flow Transition

The CERANS code with LCTM is validated for several standard (2D and 3D) test cases to evaluate its performance for flows ranging from low subsonic to hypersonic conditions involving wide range of turbulence intensities.

Flat Plate Transition Flows

Schubauer and Klebanoff Subsonic Case

Schubauer and Klebanoff test case [20, 21] is a standard zero pressure gradient, natural transition, flat plate experimental study used for validating transition models. The flow is subsonic with a Mach number of 0.147 corresponding to a freestream velocity of 50.1 m/sec, unit Reynolds number of 3.4 million, and turbulence intensity of 0.187%. The freestream eddy viscosity is considered fivefold that of the laminar viscosity. The computational domain is rectangular with the flat plate at the bottom having a length of 2 m and height of 0.4 m and the grid size is 301x4x101 amounting to 0.12 million cells. The first near wall cell spacing is 0.27 micron which correspond to a Y+ of about 0.1, 0.02 and 0.04 respectively at the leading edge, along the laminar and turbulent zones. For all the flat plate test cases, involving subsonic, supersonic and hypersonic flows, the same grid is used. In order to simulate this incompressible flow test case, Roe's flux function formulae with Thornber's correction [22] is used.

The zoomed view of computational grid is shown in Fig.1. From Mach contours shown in Fig.2, it can be observed that till a distance of 0.9 m, flow gradients are confined to a narrow region away from wall in the boundary layer, in contrast to downstream region where the gradient spread wide across depicting a thick boundary layer due to triggering of turbulence. The intermittency contours are shown in Fig.3. It shall be observed that the intermittency value is very small in the region close to wall till 0.9 m distance due to suppression of turbulence by LCTM, and is unity elsewhere. The distribution of skin friction coefficient against the streamwise Reynolds number is shown in Fig.4, along with comparison from the experimental data [20] and the laminar prediction. CERANS-LCTM code is able to predict the transition zone as well as the magnitude of skin friction very well and the comparison with experiment is very good.

Shutts Supersonic Case

In the test case due to Shutts et al. (adapted from Ref.[21]), the freestream Mach number is 2.25, temperature is 169.4 K, turbulence intensity is 0.874%, which correspond to nearing bypass transition environment and turbulence viscosity is 8.72 times laminar viscosity. Unit Reynolds number of 9 million considered in this study corresponds to that was used by Kaynak et al. [21] and the wall condition is adiabatic. The modified Roe flux function, Roe-M2, due to Kim et al. [23] is used for modeling the convective fluxes.

The Langtry-Menter correlations for, F_{length}, the transition length function and $Re_{\theta c}$, the transition critical momentum thickness Reynolds number appearing in the source terms of LCTM are valid for low speed flows. Since for high supersonic flow regime, dependence of F_{length} on $Re_{\theta t}$ is weak, the correlation due to Medida et al. [17] as a function of Tu_∞ given below is used.

$$F_{length} = 0.171\ Tu_{\infty}^{2} - 00083\ Tu_{\infty} + 0.0306$$

In this test case, the value of F_{length} is 0.154 and the expression for zero-pressure gradient $Re_{\theta t_{\infty}}$ due Langtry-Menter is retained here, equal to 658. The results obtained are presented in Figs.5 to 7. The laminar and turbulent zones are clearly distinguished as depicted in the Mach contours (Fig.5) with flow transition taking place at around 0.4 m, and the boundary layer thickens downstream of 0.4 m. The intermittency contours shown in Fig.6 clearly depict the laminar pocket contained within an entire turbulent zone. The variation and trend of the transition quantities is observed similar to that of Kaynak et al. [21].

Comparison of predicted skin friction coefficient with literature is shown in Fig.7. For Re(x) up to 3.5 million, C_f variation depict the laminar trend reaching a value of 0.0005, then with a bypass transition, increases to 0.0025 at Re(x) of 4 million, before reaching a steady asymptotic value of about 0.0020 at Re(x) of 10 million. The C_f variation purely due to laminar and SST turbulent simulations are also plotted and it can be observed that the transition C_f overshoot the turbulent C_f value during transition by an incremental value of 0.0005 and continue downstream with the same increment. However C_f variation due to transition prediction overlaps with laminar data till transition. Present prediction corroborates well with transition simulation due to Kaynak et al. [21] in terms of transition location and the increase in C_f value due to transition, though the present value is higher by about 0.0004. Incidentally, the trend of C_f variation resembles closer to the DNS data due to Gatski et al. [24] than that due to Kaynak et al. [21] as can be observed from Fig.7. From this study, it shall be remarked that CERANS-LCTM code is able to model the transition behavior for the supersonic case very well despite differences in terms of the integrated transition correlations as well as compressibility corrections used in Ref.[21] compared with.

Mee's Hypersonic Test Case

The hypersonic shock tunnel experiments performed by Mee [25] is considered for validating CERANS-LCTM using the Krause's transition correlations. The test conditions vary from low enthalpy to high enthalpy inflow conditions covering different unit flow Reynolds numbers, Mach numbers and turbulence intensities and are summarized in Table-1 [16]. The wall temperature is fixed at 600 K. Since the experiment data has an uncertainty of about 18% in the measured Stanton number [26] and the turbulence intensity of the wind tunnel is unknown, Frauholtz et al. [16] carried out an extensive parametric variation study by varying F_{length} and $Re_{\theta c}$, as well as used the in-house correlations considering different turbulence intensities, however using the differential Reynolds Stress turbulence closure model (SSG/LRR-ω) model due to Eisfeld [27]. Xia et al. [26] also varied the freestream turbulence intensity in their study for Mee's test cases, by proposing a simplified correlation model which eliminated the $R_{\theta t}$ transport equation and provided suitable correlation for $Re_{\theta c}$ within the framework of Menter's SST k-ω turbulence model. In the present study, the freestream turbulence intensity is varied around the values provided in the literature [16,26]. The consolidated Tu_{∞}, which provided best comparison with Stanton number distribution of experiment [25] is provided in Table-2 along with the values of [16,26]. Incidentally, it is observed that the Tu_{∞} of present study for which the Stanton number distribution had best agreement with the experiment data lay midway between the values used by Frauholtz et al. [16] and Xia et al. [26].

The Stanton number distribution for the four test cases are presented in Figs.8-11, along with comparison due to Frauholtz et al. [16] and experiment data. Simulation data due to laminar, fully turbulent and transition simulations are presented in these figures and it is observed that with increase in turbulence intensity the transition location moves upstream as expected. The data due to experiment is observed to have high scatter and the corroboration of

Table-1 : Flow Conditions for Hypersonic Flat Plate Transition

Test	Condition	Nozzle Enthalpy MJ/kg	M_{∞}	T_{∞} (K)	Re_{∞} / m (10^6)
1	Low Enthalpy, Low Re	5.3	6.3	570	1.7
2	Low Enthalpy, Mid Re	6.2	6.2	690	2.6
3	Low Enthalpy, High Re	6.8	6.1	800	4.9
4	High Enthalpy, Low Re	12.4	5.5	1560	1.6

Table-2 : Comparison of Freestream Turbulence Intensity (Tu_∞ %)

Test	Frauholz et al. [16]	Xia et al. [26]	Present
1	5.7	2.6	3.5
2	4.4	2.0	3.0
3	3.7	1.7	2.5
4	3.8	2.2	3.0

present simulation data for all the cases is observed to be good both in terms of magnitude of Stanton number as well as the transition Reynolds number, Re(x).

Low Subsonic Flow Past Aerospatiale-A Airfoil

The case of maximum lift low subsonic flow past Aerospatiale-A airfoil [28] is widely used for validating transition models. The flow conditions are: freestream Mach number is 0.15, Reynolds number is 2.1 million, angle of attack is 13.1 degrees and freestream turbulence intensity is 0.03 %.

The grid for this configuration is shown in Fig.12 consists of 448 points on the airfoil and 66,000 cells overall. A closer view of the airfoil depicting the C-H topology grid and clustering of points near leading/trailing edges, wall and wake is presented in Fig.13. In the experiment of Hasse et al. [28], it was observed that over the suction side, laminar boundary layer develops and terminates with a laminar separation bubble at 12% of chord around the location of suction peak, causing separation-induced transition and further develops into a turbulent boundary layer downstream [13]. The turbulent boundary layer eventually separates at the trailing edge due to large adverse pressure gradient. The CERANS-LCTM results are presented in Figs.14 to 20.

The pressure contours due to present transition flow simulation are shown in Fig.14. The low pressure zone having peak suction at the leading edge can be clearly observed. C_p distribution presented in Fig.15 depict a very good comparison with experiment and the suction peak value is about 4.2. The Mach contours in Fig.16 show the trailing edge separation and the turbulent wake aft of trailing edge is shown in the eddy viscosity contours in Fig.17. The attached laminar boundary layer at the suction side leading edge till the zone of flow transition, and further turbulence downstream of the suction peak shall be observed from the intermittency contours in Fig.18. The $R_{\theta t}$ contours in Fig.19 depict low $R_{\theta t}$ at high pressure gradient regions and vice versa as expected.

In the plot of skin friction distribution, C_f, shown in Fig.20, it shall be observed that the flow separation and hence negative values of skin friction is completely missed out by the present simulation, though, a region of low near wall velocity with high traction and near incipient profiles, leading to near zero C_f are observed. The skin friction prediction by Medida et al. [17] clearly depict a small laminar separation bubble as can be observed in the C_f distribution. However in the present simulation, the transition model was able to suppress turbulence till the suction peak by maintaining laminar flow, and further mimicking the separation induced transition, predicting a sharp rise in skin friction value at around 11% of chord. Further downstream of this location, C_f distribution exactly follow the profile of experimental data. The main reason for missing laminar separation bubble by present simulation shall be attributed to extending applicability range of density based CERANS solver to handle low Mach number, incompressible, high angle of attack flow. Barring this shortcoming, the overall predictability of flow transition is encouraging.

Hypersonic Transitional Flow Over Sharp Cone

The geometry is a sharp cone with 7 degree half-cone-angle, having a length of 1.0 m. The transition data for comparison is sourced from the extensive experimental results of Kimmel et al. presented in the doctoral thesis dissertation of McKeel et al. [29]. Structured grid for the geometry consists of 101 points in both streamwise and wall normal directions and 33 points along the circumference, amounting to 0.32 million cells. The surface grid is shown in Fig.21 and the grid in pitch plane is shown in Fig.22. The first near wall cell spacing is 1.5 micron which yielded a minimum Y^+ of 0.03 and a maximum of 0.24.

The flow conditions for transition simulation are Mach number 7.93, Reynolds number 6.6 million/m, freestream temperature 53.18 K, freestream density 0.0197 kg/m^3 and wall temperature 303.24K. AUSM-PW+ numerical scheme is considered for evaluation of convective fluxes, freestream turbulence intensity is 2.5%, freestream turbulent viscosity ratio is 0.01 and transition correlation due to Krause et al. [16] is considered. Since the input data of freestream turbulence intensity and eddy viscosity ratio are not available in the references, it was required to make

some numerical experiments by varying these parameters, before arriving at the presently held values.

The pressure contours are shown in Fig.23 depicting the conical shock. Average surface pressure on the cone is about 2.7 times the freestream pressure and the corresponding SIMS cone table value is 2.54. Eddy viscosity ratio contours are shown in Fig.24, and it clearly depict the transition onset. Plot of surface heat transfer coefficient (Stanton number), C_h, and comparison with literature is shown in Fig.25. Transition simulation data is compared with experiment data due to Kimmel [29] and the laminar and turbulent results are compared with CFD data to McKeel [29]. It can be clearly observed that the laminar as well as turbulent heat transfer coefficient distributions are in very good agreement with literature.

In case of transition simulation, the overall trend such as, location of transition onset and incremental heat flux due to flow transition are predicted with good accuracy. The post-transition C_h data due to present simulation breach the fully turbulent data and attain higher values, closer to experiment data. However, the transition length due to the present simulation is higher than the experiment data by about 28%, which is due to shallow slope of Ch in transition zone. Deviation of C_h distribution, though only marginal, is mainly attributed to the generalized extension of 2D flat plate hypersonic transition correlations of [16] as such for 3D sharp cone hypersonic flow, without any modifications. It is an acknowledged fact that different transition correlations predict widely varying C_h distributions in hypersonic transitional flows, and hence necessitates careful investigation and calibration of the known correlations used in the LCTM framework. Despite the above limitation, the overall superior predictive capability of CERANS LCTM for 3D hypersonic transition flow is demonstrated.

Conclusions

The two equation $\gamma - Re_{\theta_t}$ local correlation based transition model is implemented in CERANS code and validated for several transition problems available in literature covering speed range from low subsonic to hypersonic conditions. Overall, comparison of flow transition results with literature data is observed to be very good. Based on the wide range validation studies, the prospect of $\gamma - Re_{\theta_t}$ LCTM as a general purpose transition prediction tool is ascertained effectively despite acknowledging the dependency of the model solely on local correlations for all modes of transition. It is necessary to further extend the validity range of CERANS-LCTM to non-zero pressure gradient flows as well as to more hypersonic test cases with flow separation for increasing the confidence level and reliability. Further it is necessary to implement the cross-flow transition correlations for addressing high angle of attack 3D transitional flows, and shall complete the wider scope of transition modeling in CERANS.

References

1. Di Pasquale, D., Rona, A. and Garrett, S. J., "A Selective Review of CFD Transition Models", 39th AIAA Fluid Dynamics Conference, 22-26 June 2009, San Antonio, Texas, AIAA 2009-3812.

2. Tapan K. Sengupta., "Theoretical and Computational Aerodynamics", Wiley Aerospace Series, First Edition, Published by John Wiley and Sons Ltd, 2015.

3. Dhawan, D. and Narasimha, R., "Some Properties of Boundary Layer Flow During Transition from Laminar to Turbulent Motion", Journal of Fluid Mechanics, Vol.3, pp.418-436, 1958.

4. Abu-Ghannam, B.J. and Shaw, R., "Natural Transition of Boundary Layers - the Effects of Turbulence, Pressure Gradient and Flow History", Journal of Mechanical Engineering Science, Vol.22, No.5, pp.213-228, 1980.

5. Mayle, R.E., "The Role of Laminar-turbulent Transition in Gas Turbine Engines", Journal of Turbomachinery, Vol.113, pp.509-537, 1991.

6. Suzen, Y.B. and Huang, P.G., "Model of Flow Transition Using and Intermittency Transport Equation", Journal of Fluid Engineering, Vol.122, pp.273-284, 2000.

7. Suzen, Y., Xiong, G. and Huang, P., "Prediction of Transitional Flows in low-pressure Turbines Using an Intermittency Transport Equation", AIAA Journal, Vol.40, No.2, pp.254-266, 2002.

8. Wilcox, D.C., "Simulation of Transition with a Two-equation Turbulence Model", AIAA Journal, Vol.32, No.2, 1994.

9. Walters, D.K. and Leylek, J.H., "A New Model for Boundary Layer Transition Using a Single Point

RANS Approach", Journal of Turbomachinery, Vol.126, pp.193-202, January 2004.

10. Steelant, J. and Dick, E., "Modeling of Bypass Transition with Conditioned Navier-Stokes Equations Coupled to Intermittency Transport Equations", Int. J. Numer. Methods Fluids, Vol.23, pp.193-220, 1996.

11. Papp, J. L. and Dash, S. M., "A Rapid Engineering Approach to Modeling Hypersonic Laminar to Turbulent Transitional Flows for 2D and 3D geometries", 15th AIAA International Space Planes and Hypersonic Systems and Technologies Conference, AIAA Paper 2008-2600, 2008.

12. Langtry, R. B. and Menter, F. R., "Correlation-based Transition Modeling for Unstructured Parallelized Computational Fluid Dynamics Codes", AIAA Journal, Vol.47, No.12, pp.2894-2906, 2009.

13. Langtry, R.B., "A Correlation-based Transition Model Using Local Variables for Unstructured Parallelized CFD Codes", Ph.D. Thesis, University of Stuttgart, 2006.

14. Menter, F., "Two-equation Eddy Viscosity Turbulence Models for Engineering Applications", AIAA Journal, Vol.32, No.8, pp.1598-1605, 1994.

15. Krause, M., Behr, M. and Ballmann, J., "Modeling of Transition Effects in Hypersonic Intake Flows Using a correlation-based Intermittency Model", 15th AIAA International Space Planes and Hypersonic Systems and Technologies Conference, Dayton, Ohio, AIAA 2008-2598, April-May 2008.

16. Frauholz, S., Reinartz, B.U., Muller, S. and Behr, M., "Transition Prediction for Scramjets Using $\gamma - Re_{\theta_t}$ Model Coupled to Two Turbulence Models", Journal of Propulsion and Power, Vol.31, No.5, pp.1404-1415, September-October 2015.

17. Medida, S. and Baeder, J.D., "Application of the Correlation-based $\gamma - Re_{\theta_t}$ Transition Model to the Spalart-Allmaras Turbulence Model", 20th AIAA Computational Fluid Dynamics Conference, AIAA 2011-3979, Honolulu, HI, June 2011.

18. Balasubramanian, R. and Anandhanarayanan, K., "Viscous Computations for Complex Flight Vehicles Using CERANS with Wall Function", CFD Journal, Vol.16. No.4, pp.386-390, 2008.

19. Spalart, P.R. and Allmaras, S.R., "A One Equation Turbulence Model for Aerodynamic Flows", 30th Aerospace Sciences Meeting and Exhibit, AIAA Paper 92-0439, Reno, NV, 1992.

20. Schubauer, G.B. and Klebanoff, H.K., "Contribution on the Mechanics of Boundary Layer Transition", NACA TN 3489, 1955.

21. Kaynak, Ü., "Supersonic Boundary-layer Transition Prediction Under the Effect of Compressibility Using a Correlation Based Model", Proceedings of the Institution of Mechanical Engineers, Part G: Journal of Aerospace Engineering, Vol.226, No.7, pp.722-739, June 2012.

22. Thornber, B., Mosedale, A., Drikakis, D., Youngs, D. and Williams, R.J.R., "An Improved Reconstruction Method for Compressible Flows with Low Mach Number Features", Journal of Computational Physics, Vol.227, pp.4873-4894, 2008.

23. Kim, S.S., Kim, C., Rho, O.H. and Hong, S.K., "Cures for Shock Instability: Development of a Shock-stable Roe Scheme", Journal of Computational Physics, Vol.185, pp.342-374, 2003.

24. Gatski, T. B. and Erlebacher, G., "Numerical Simulation of a Spatially Evolving Supersonic Turbulent Boundary Layer", NASA/ TM-2002-211934, 2002.

25. Mee, D., "Boundary-layer Transition Measurements in Hypervelocity Flows in a Shock Tunnel", AIAA Journal, Vol.40, No.8, pp.1542-1548, 2002.

26. Xia Chenchao and Chen Weifang., "Boundary-layer Transition Prediction Using A Simplified Correlation-based model", Chinese Journal of Aeronautics, Vol.29, No.1, pp.66-75, 2016.

27. Eisfeld, B., "Advanced Turbulence Modeling and Stress Analysis for the DLR-F6 Configuration", 23rd

AIAA Applied Aerodynamics Conference, Toronto, Ontario Canada, AIAA 2005-4727, June 2005.

28. Haase, W., Chaput, E., Elsholz, E., Leschziner, M. and Mueller, U.R, "ECARP- European Computational Aerodynamics Research Project: Validation of CFD Codes and Assessment of Turbulence Models", Notes on Numerical Fluid Mechanics, Vol.58, 1997.

29. McKeel, S.A., "Numerical Simulation of the Transition Region in Hypersonic Flow", Ph.D Thesis, Aerospace Engineering, Virginia Polytechnic Institute and State University, Blacksburg, Virginia, February 1996.

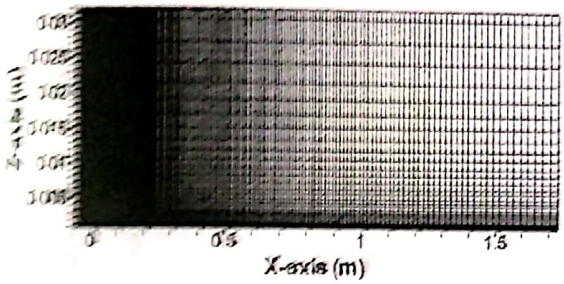

Fig.1 Grid for Subsonic Flat Plate

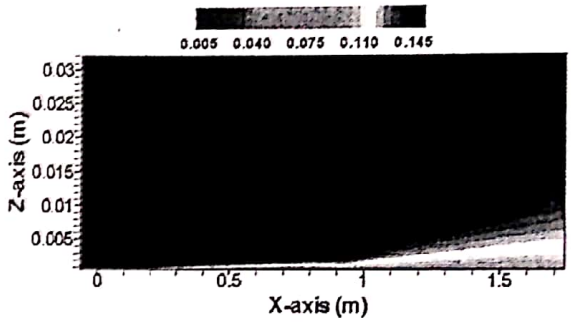

Fig.2 Mach Contours

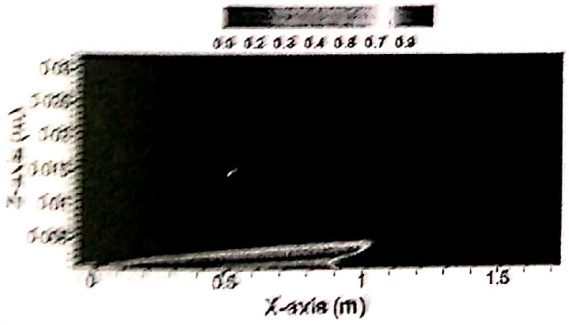

Fig.3 Intermittency 'γ' Contours

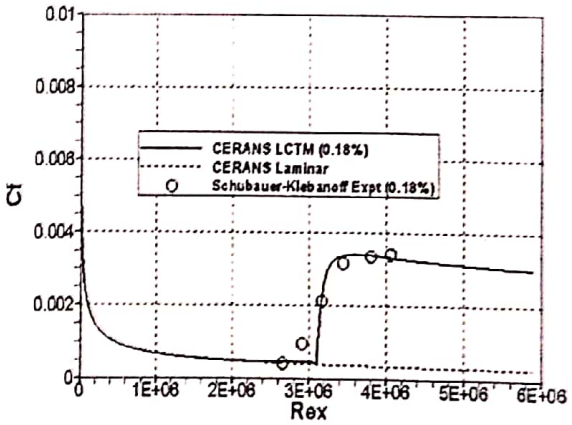

Fig.4 Cf Distribution

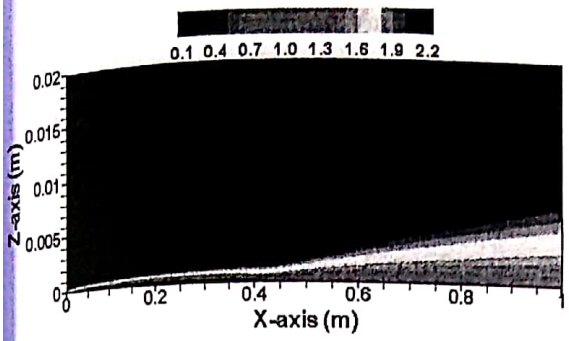

Fig.5 Mach Contours (Supersonic)

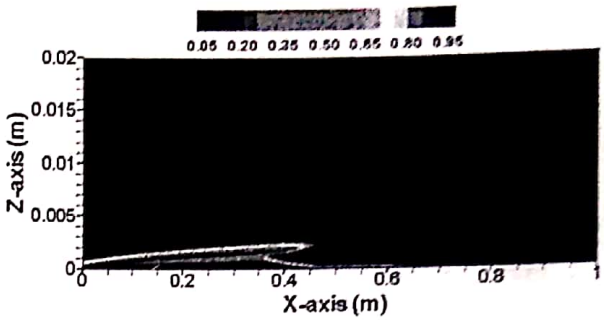

Fig.6 Intermittency 'γ' Contours (Supersonic)

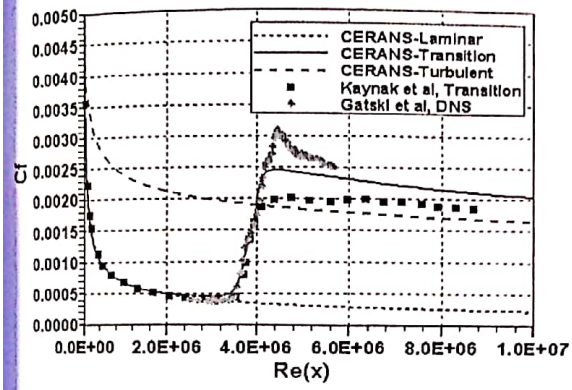

Fig.7 C_f Distribution (Supersonic)

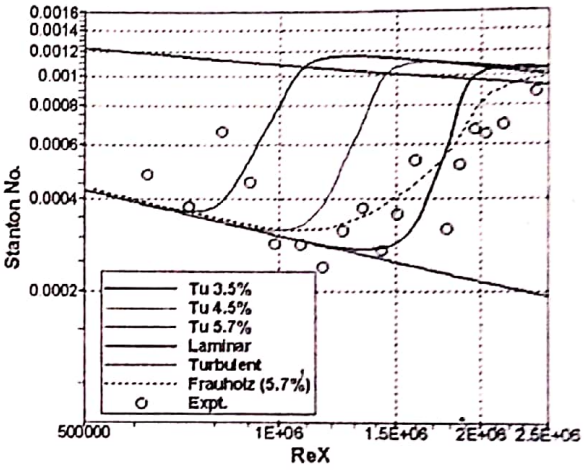

Fig.8 St vs Re(x) : Case 1, Mach 6.3

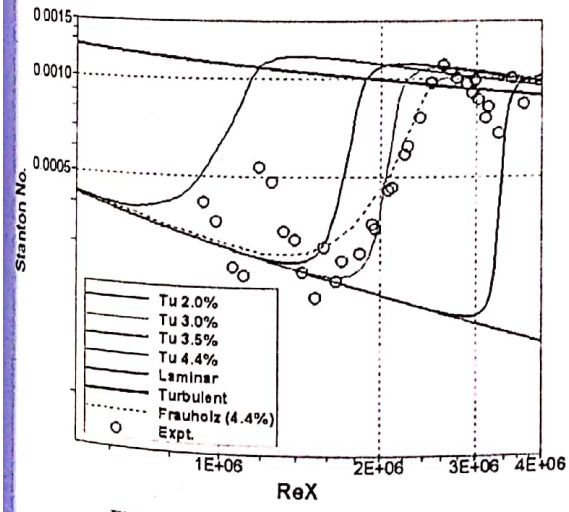

Fig.9 St vs Re(x) : Case 2, Mach 6.2

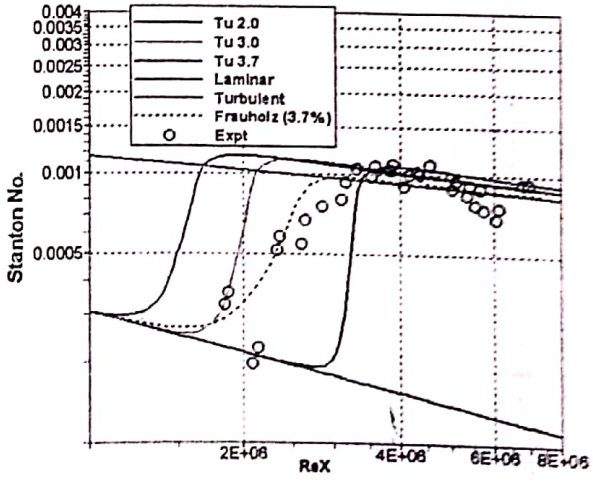

Fig.10 St vs Re(x) : Case 3, Mach 6.1

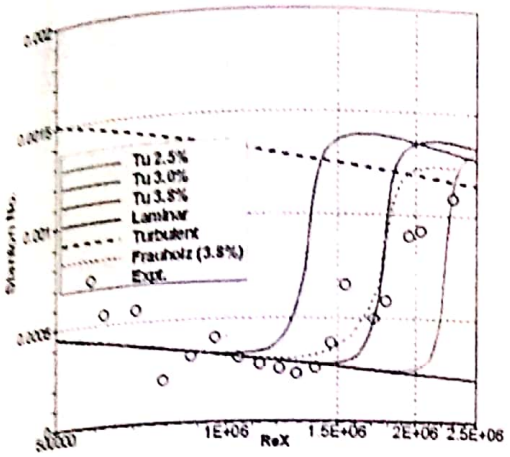

Fig.11 St vs Re(x) : Case 4, Mach 5.5

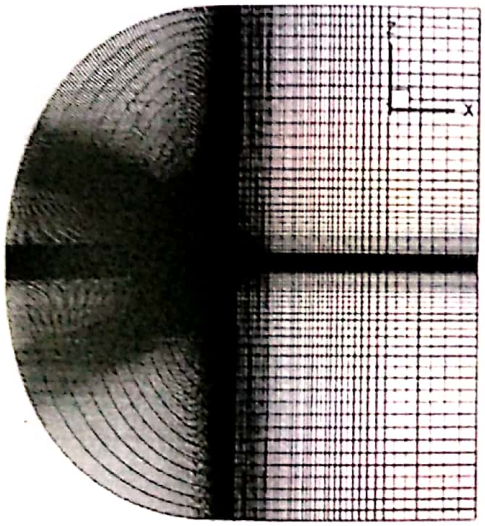

Fig.12 Aerospatiale-A Grid

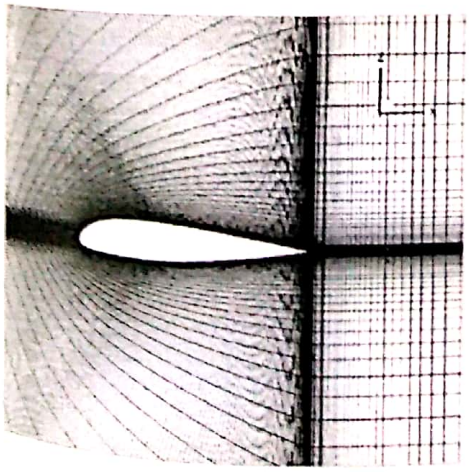

Fig.13 Grid Near Airfoil

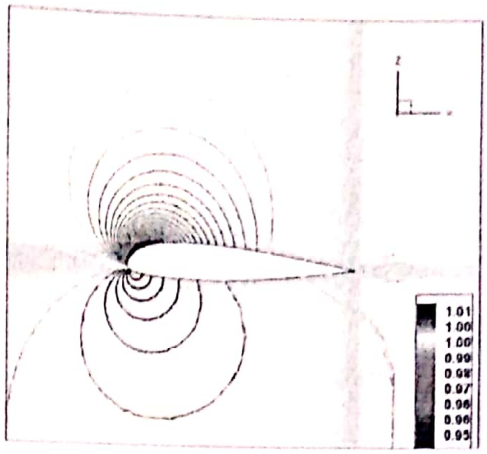

Fig.14 Pressure Contours (p/p_∞)

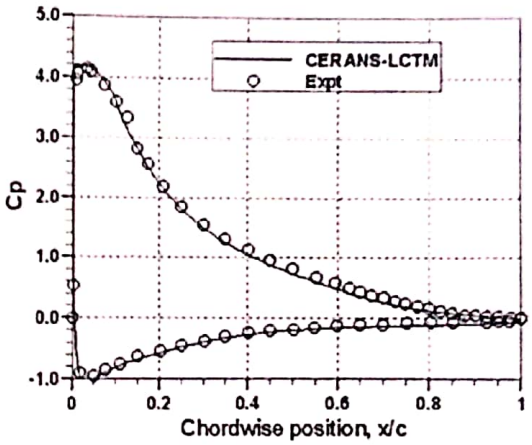

Fig.15 C_p Distribution

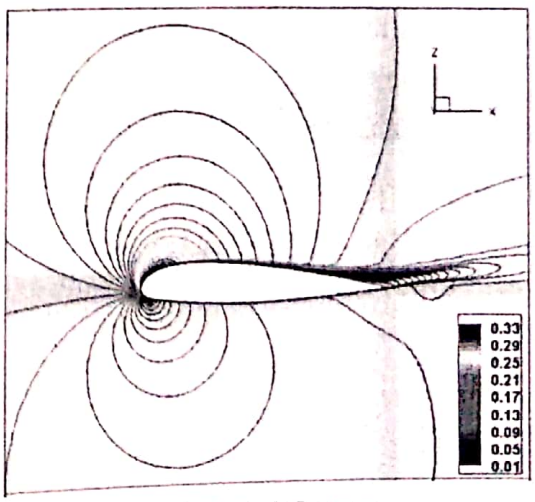

Fig.16 Mach Contours

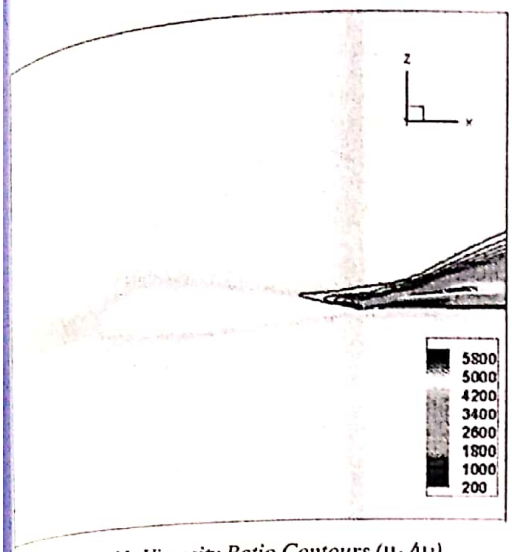

Fig.17 Eddy Viscosity Ratio Contours (μ_t/μ_l)

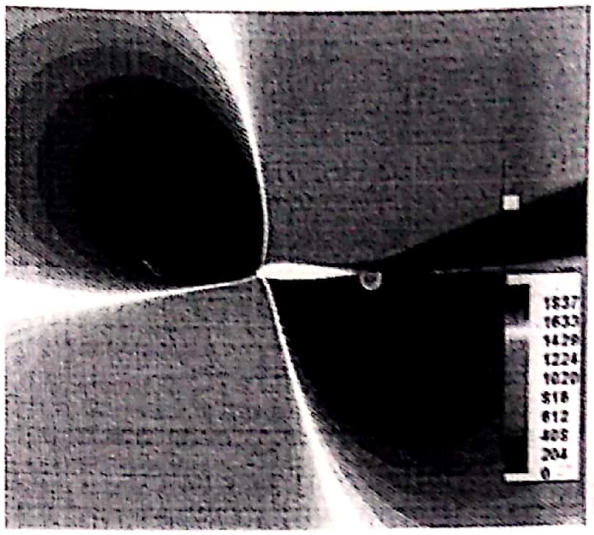

Fig.19 Re_θ Contours

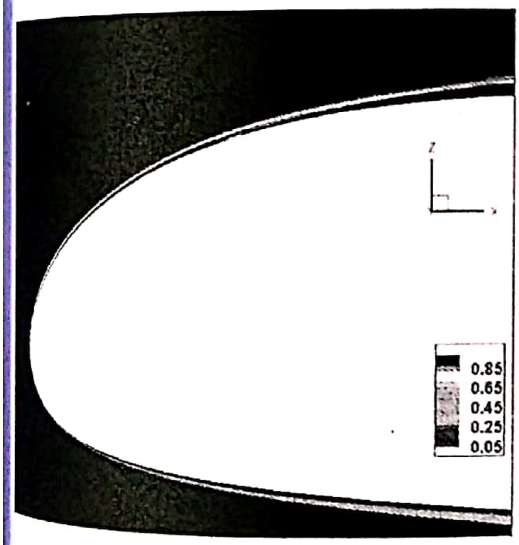

Fig.18 Intermittency 'γ' Contours at L.E.

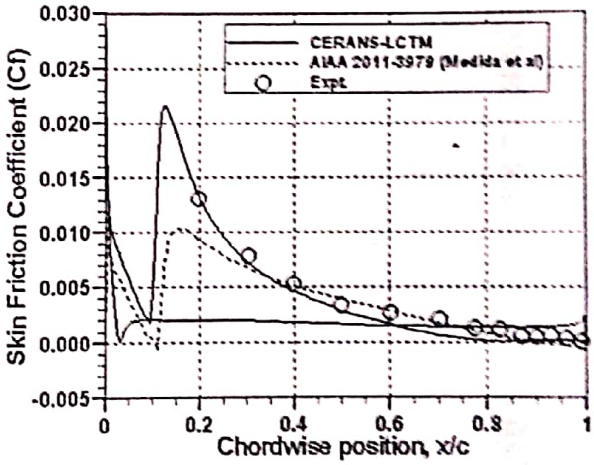

Fig.20 Skin Friction Distribution

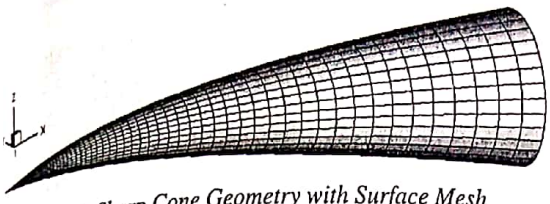

Fig.21 Sharp Cone Geometry with Surface Mesh (7° Half Cone Angle)

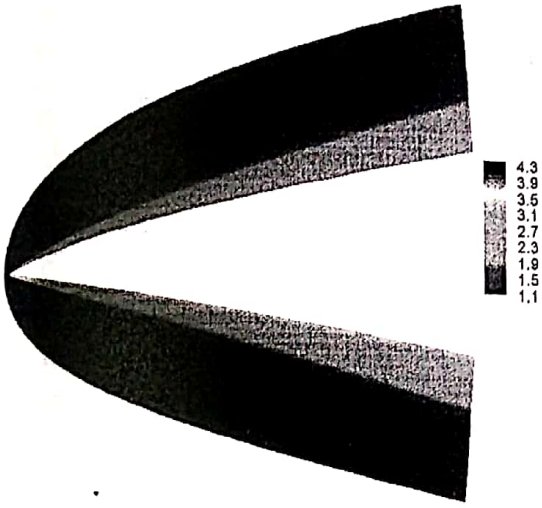

Fig.23 Pressure Contours (p/p_∞)

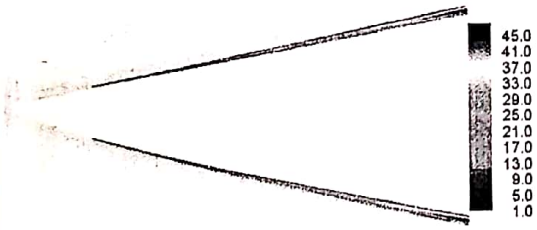

Fig.24 Eddy Viscosity Ratio Contours (μ_t/μ_l)

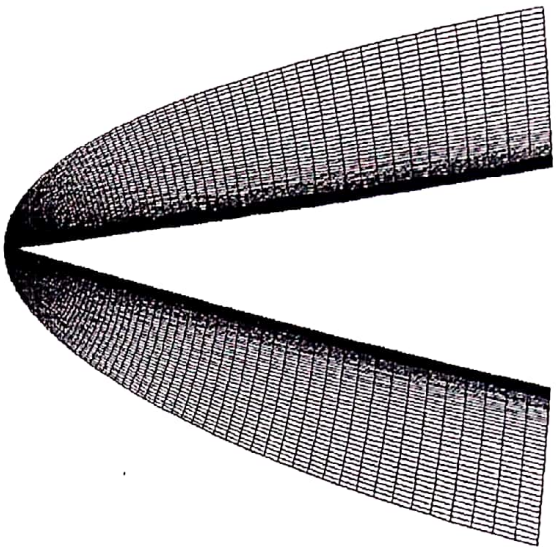

Fig.22 Grid in Pitch Plane

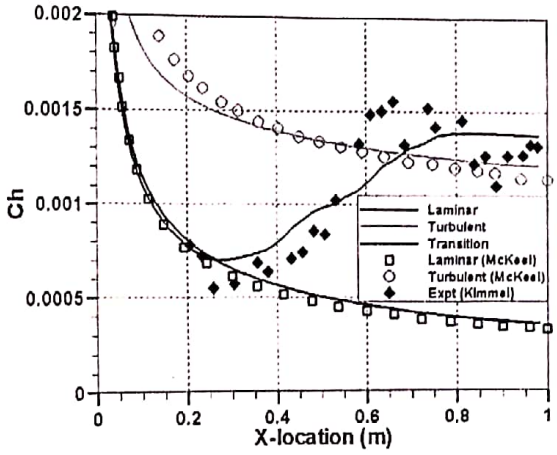

Fig.25 Comparison of Surface Heat Transfer Coefficient